Single-Stand Polarimetric Response and Calibration

Steve Ellingson*

June 15, 2008

Contents

*Bradley Dept. of Electrical & Computer Engineering, 302 Whittemore Hall, Virginia Polytechnic Institute & State University, Blacksburg VA 24061 USA. E-mail: ellingson@vt.edu

1 Summary

This memo addresses the polarimetric response and calibration of LWA antenna stands, considered one at a time in isolation (i.e., without mutual coupling). As described in LWA Memo 119 ("Long Wavelength Array Station Architecture") [1], an LWA antenna stand consists of two orthogonal "inverted-vee" dipole antennas mounted above a ground screen.[1] The terminals of each dipole are interfaced to a coaxial cable using an "active balun." The cable connecting each active balun to the electronics shelter has length on the order of 150 m. Inside the electronics shelter, each signal is separately digitized and converted from the raw linear polarizations to calibrated orthogonal circular polarizations. This processing is to be done simultaneously and coherently over the entire bandwidth of interest; i.e., at least 20–80 MHz. Finally, the calibrated circulars are to be combined to form full-bandwidth beams. There is also interest in implementing an all-sky imaging capability (for example, using the "TBW" capability described in [1]) for which the efficacy of polarization calibration has significant implications.

The procedure for full-bandwidth conversion of the raw linear polarizations delivered to the shelter to the orthogonal circular polarizations desired for beamforming is complicated by several factors. First, all candidate antenna designs have axial ratios which vary significantly with respect to both frequency and direction [2]; thus the optimal polarization conversion is both frequency- and angle-dependent. Second, it is known that candidate antennas and cables exhibit significant dispersion over the frequency range of interest [3, 4]. Although the FIR-filter-based polarization calibration scheme described in LWA Memo 106 [5] can in principle manage all of these factors and deliver arbitrarily precise calibration, it has not previously been known how many taps would be required for the FIR filters in order to achieve acceptable performance, and the extent to which a precise calibration for any one direction (e.g., the zenith) would be acceptable for directions far from this nominal direction (e.g., low elevations). The former question impacts the sizing (hence, cost and power consumption) of FPGAs, whereas the latter question speaks to possible constraints on the useable simultaneous field of view, and hence maximum angular separation of full-bandwidth beams, due to polarization error. This memo attempts to answer these questions.

Principal findings are as follows:

- It is observed that antennas are in fact dispersive in two different ways: As a result of impedance mismatch (as has already been noted in [3]) and also as result of varying current distribution as a function of frequency. The latter was not previously recognized, but is significant.
- It appears there is no fundamental difficulty in implementing arbitrarily precise calibration, assuming FIR filters of sufficient length and assuming that the calibration coefficients are readily available via simulations or measurements. Practical methods for obtaining the calibration coefficients (using for example astronomical sources or artificial beacons) are not addressed in this memo, but is the topic of several planned future tasks.
- FIR filters consisting of $M = 16$ complex-valued coefficients arranged as shown in Figure 1 of LWA Memo 106 is suggested as an appropriate tradeoff between performance and FPGA requirements (cost and power consumption), assuming 98 MSPS data streams. This takes into account conversion of raw linears to pure circulars as well as variable phase and dispersion due to antennas and cables. For this choice of M applied to directions 74° from the zenith, magnitude and phase errors are less than 10% and 10° respectively, and cross-pol rejection is better than 15 dB over most of the frequency range of interest. Performance improves dramatically with decreasing zenith angle. As expected, much better performance can be achieved by using more taps, and the same level of performance can be achieved over a smaller frequency range using a smaller number of taps.

[1] At present, no further details of the antenna design have been settled.

- As expected, polarization calibration is more robust for directions near zenith as opposed to those at low elevations. For example, for a given M, better performance is obtained near the zenith than at lower elevations.
- The optimal calibration coefficients are direction dependent. However, it is found that a calibration solution obtained for the zenith degrades gracefully with increasing zenith angle and is still relatively good 30° away. Performance degrades badly between 45° and 60° and is probably completely unacceptable at 74°. No attempt has been made to assess the degradation of polarization calibration over the field of view of a beam, which could be an issue for lower-elevation beam pointings.

2 Response Model

This section describes the model that is used to calculate the frequency and polarimetric response of the antenna-cable signal path for subsequent sections.

A single antenna can be modeled as a circuit consisting of a voltage source V_A in series with the antenna impedance Z_A. For a single incident plane wave expressed in terms of the electric field $\mathbf{E}^i(\hat{\mathbf{r}})$ incident from direction $\hat{\mathbf{r}}$, V_A is given by

$$V_A = \mathbf{E}^i(\hat{\mathbf{r}}) \cdot \mathbf{l}(\hat{\mathbf{r}}) \tag{1}$$

where $\hat{\mathbf{r}}$ points from the antenna terminals toward the direction of incidence. $\mathbf{l}(\hat{\mathbf{r}})$ has units of length and is therefore known as the vector effective length (VEL). VEL conveys the same information as polarimetric pattern data, but is somewhat more convenient in the present analysis. VEL can be determined from reciprocity, by applying a test current I_{t0} to the terminals and observing the resulting current distribution. The VEL for any wire antenna is given by

$$\mathbf{l}(\hat{\mathbf{r}}) = \frac{1}{I_{t0}} \int_{wire} I_t(l) \hat{\mathbf{p}}(l) \times \hat{\mathbf{r}} \times \hat{\mathbf{r}} \; e^{-jk\mathbf{w}(l)\cdot\hat{\mathbf{r}}} \; dl \tag{2}$$

where $I_t(l)$ is current resulting from the application of I_{t0} to the terminals, l is arclength along the wire defining the antenna, $\mathbf{w}(l)$ is the coordinates of the wire at position l, and $\hat{\mathbf{p}}(l)$ is the unit tangent the the wire at position l. It should be noted that the VEL concept is completely general, and moreover Equation 2 can be applied to any antenna which can be modeled as wire grid; e.g., to blade antennas and other LWA candidate antennas.

Consider the two orthogonal dipoles making up an LWA stand. Let us assume one of these dipoles is aligned along the x-axis of a Cartesian coordinate system, and that the other is aligned along the y-axis. The z-axis points to the zenith. Let the associated VELs for these dipoles be $\mathbf{l}_x(\hat{\mathbf{r}})$ and $\mathbf{l}_y(\hat{\mathbf{r}})$ respectively. Note $\mathbf{E}^i(\hat{\mathbf{r}})$ can always be decomposed into a component of left-circular polarization (LCP) E_L and a component of right-circular polarization (RCP) E_R. Then we know from LWA Memo 106 that the antenna terminal open-circuit voltages are given by

$$\begin{bmatrix} V_x \\ V_y \end{bmatrix} = \begin{bmatrix} (\hat{\mathbf{a}} \cdot \mathbf{l}_x) & (\hat{\mathbf{b}} \cdot \mathbf{l}_x) \\ (\hat{\mathbf{a}} \cdot \mathbf{l}_y) & (\hat{\mathbf{b}} \cdot \mathbf{l}_y) \end{bmatrix} \begin{bmatrix} 1 & 1 \\ j & -j \end{bmatrix} \begin{bmatrix} E_L \\ E_R \end{bmatrix} \tag{3}$$

where $\hat{\mathbf{a}}$ and $\hat{\mathbf{b}}$ are any two orthogonal unit vectors transverse to the direction of incidence ($\hat{\mathbf{r}}$). A convenient choice is:

$$\hat{\mathbf{b}} = \frac{\hat{\mathbf{x}} \times \hat{\mathbf{r}}}{|\hat{\mathbf{x}} \times \hat{\mathbf{r}}|} \tag{4}$$

$$\hat{\mathbf{a}} = \hat{\mathbf{b}} \times \hat{\mathbf{r}} \tag{5}$$

Once the antenna is connected to the active balun, the input impedance of the active balun Z_L appears in series with the antenna impedance Z_A. Thus the voltage delivered to the active balun

is less than the open circuit antenna voltage according to the voltage divider $Z_L/(Z_A + Z_L)$. We shall assume that the active balun is utterly frequency-independent and has unity gain; the former is justified on the basis that the frequency dependence of candidate active baluns is known to be very slight compared to the other factors of interest in this study, and the latter is justified on the basis that we are not interested in the present study in factors which do not vary significantly between antennas.

The coaxial cable, on the other hand, is both significantly frequency-dependent and potentially variable from stand to stand. The appropriate transfer function is $e^{\gamma d}$ where γ is the propagation constant defined in Equation (12) of LWA Memo 136 [4] and d is the length of the cable. Note that this expression captures all relevant cable effects including frequency-dependent attenuation, phase, and dispersion. However, the "ideal" part of the frequency-dependent phase, representing dispersion-free delay associated with cable length, is not of interest in the calibration process being considered here, and is in that sense a nuisance parameter as it varies quickly as a function of frequency. This portion of the cable response is given by $e^{-j\beta_0 d}$ where $\beta_0 = \sqrt{\mu_0 \epsilon_r \epsilon_0}$ where μ_0 and ϵ_0 are the permeability and permittivity, respectively, of free space; and ϵ_r is the relative permittivity of the dielectric spacing material used in the cable.

Thus the complete response model used in this study is:

$$\begin{bmatrix} \tilde{V}_x \\ \tilde{V}_y \end{bmatrix} = \frac{e^{-\gamma d}}{e^{-j\beta_0 d}} \frac{Z_L}{Z_A + Z_L} \begin{bmatrix} (\hat{\mathbf{a}} \cdot \mathbf{l}_x) & (\hat{\mathbf{b}} \cdot \mathbf{l}_x) \\ (\hat{\mathbf{a}} \cdot \mathbf{l}_y) & (\hat{\mathbf{b}} \cdot \mathbf{l}_y) \end{bmatrix} \begin{bmatrix} 1 & 1 \\ j & -j \end{bmatrix} \begin{bmatrix} E_L \\ E_R \end{bmatrix} \tag{6}$$

where the tilde over V_x and V_y is used to indicate that these represent the raw polarizations delivered to the calibration processor, subject to the caveats and modifications explained in the above paragraphs.

3 Expected Polarimetric and Frequency Response of an LWA Antenna Stand

To better understand what can be expected from an LWA stand and its associated cabling, an example is presented here. The antenna considered here is a simple thick-wire inverted-vee dipole, modeled using NEC-2. A thick-wire antenna is chosen as opposed to a blade-type antenna because it is simple and less likely to be subject to anomalies resulting from NEC-related issues. The tradeoff is that this antenna has considerably less bandwidth from an impedance matching perspective. This is not entirely bad as the frequency-domain calibration results can thus be interpreted as conservative.

The details of the antenna are completely defined in the NEC-2 input file included in Appendix A. Each dipole has a total length of 4.0753 m, radius of 15 mm, and is bent downward at a 45° angle. The vertex of each antenna is about 1.5 m above an infinite ground plane. In the NEC model, the orthogonal dipole is always present and is loaded with 100 Ω at the feedpoint. The NEC model is run just once, with the antenna of interest driven by a voltage source. This yields the currents along the length of the antenna, including at the feedpoint, from which the antenna impedance and VEL can be calculated.

The cable is assumed to be 150 m of RG58, using the constitutive parameters given in Section 4 of LWA Memo 136 [4].

Figure 1 shows the open-circuit antenna response to a signal incident from the zenith. This could also be interpreted as the voltage at the input of an active balun with very large input impedance. The response is expressed in terms of the magnitude and phase of the effective length, since this literally the transfer function from electric field (V/m) to voltage. Magnitude is expressed in terms of dB relative to 1 m. It is interesting to note that the antenna is dispersive due to a change in phase

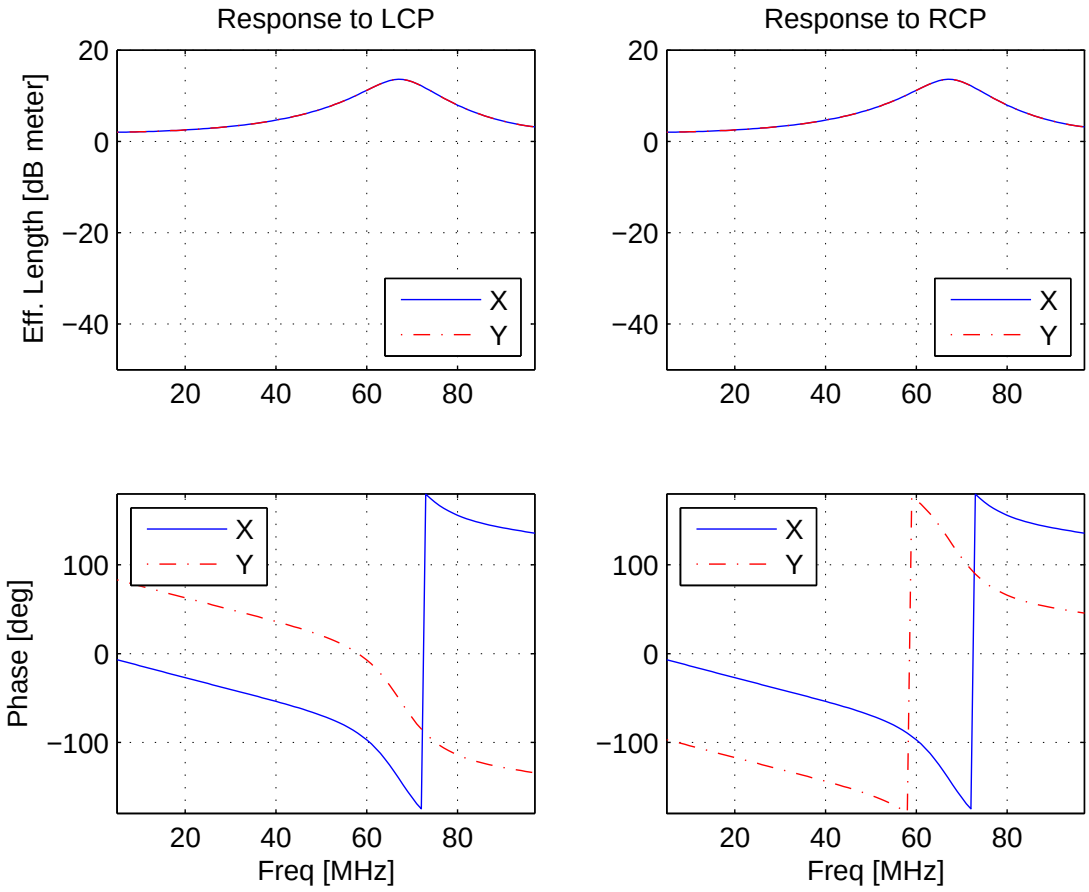

Figure 1: Zenith incidence: Open-circuit response.

slope with frequency around 65 MHz. This an additional source of dispersion independent of the dispersive mechanism identified in LWA Memo 115 [3], which was attributable to mismatch between the antenna impedance and the active balun input impedance. The new source of dispersion is attributable to the variation in time required for currents excited on different parts of the antenna to arrive at the feedpoint. Despite this, we observe the expected result that the magnitude response to LCP and RCP are identical, and that phase difference between the "x" and "y" dipoles is 90° such that pure LCP and RCP can be obtained by simply by adding the antenna outputs with the appropriate 90° phase shift. This is not affected by mismatch or cable affects (as we shall soon see), so no calibration *of polarization* is needed for zenith incidence, although calibration is needed for to correct the overall frequency response.

Figure 2 shows the response at the active balun input, assuming a 100Ω input impedance, to a signal incident from the zenith. The deleterious impact of the poor match is apparent in the decreased effective length. We also see the region of maximum dispersion is shifted from about 65 MHz to a frequency closer to resonance.

Figure 3 shows the response at the far end of the cable to a signal incident from the zenith. The cable of course results in further frequency-dependent reduction of the voltage (through attenuation), and increases the apparent dispersive delay.

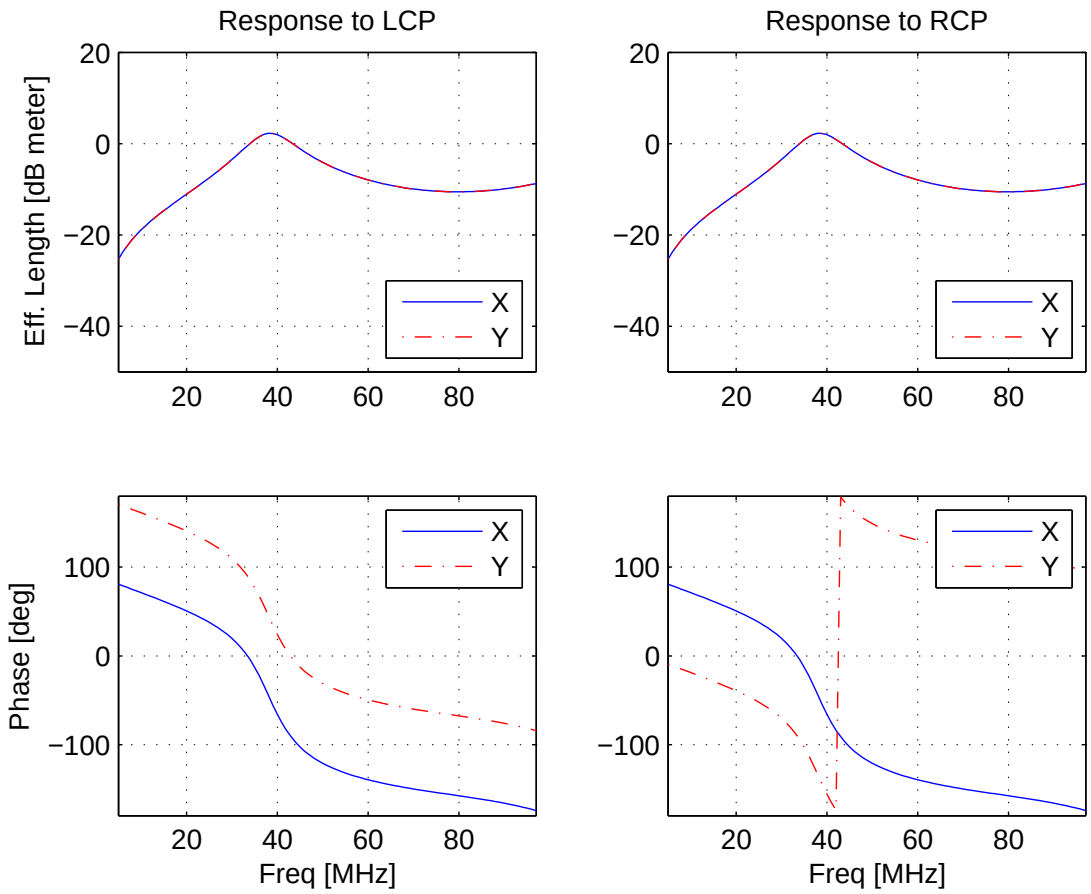

Figure 2: Zenith incidence: Active balun input.

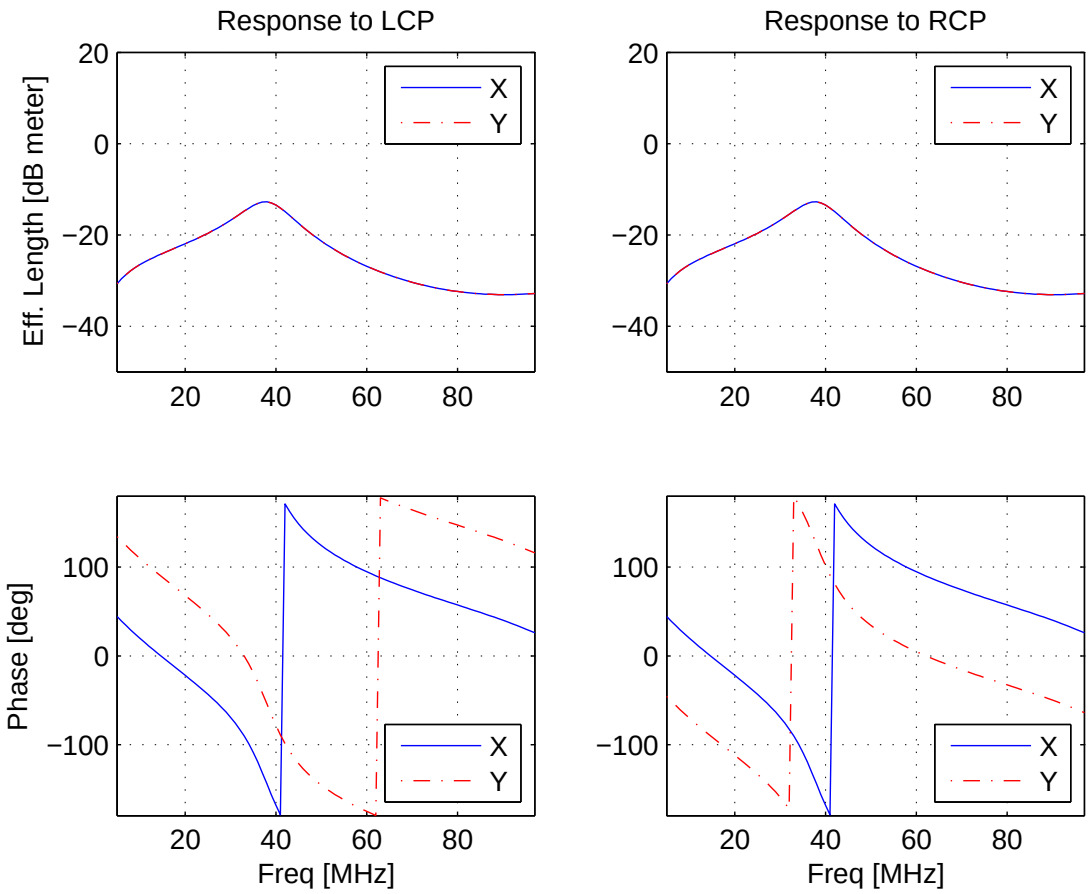

Figure 3: Zenith incidence: Cable output.

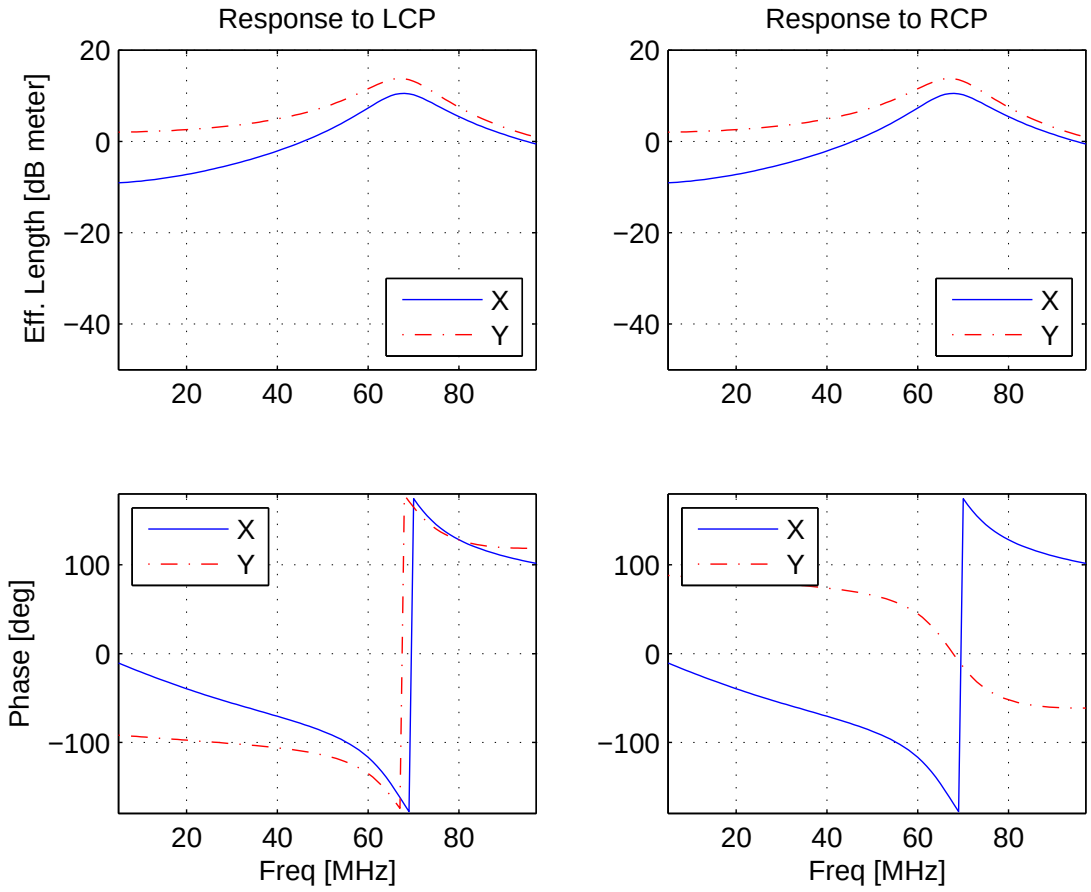

Figure 4: $\theta = 74°$, $\phi = 0$: Open-circuit response.

Figure 4 shows the open-circuit antenna response to a signal incident from $\theta = 74°$ (measured from zenith) and $\phi = 0$; i.e., along the x-axis. Here we see the x-oriented dipole is suppressed slightly compared to the y-oriented dipole, as one would expect since these dipoles are endfire and broadside, respectively, in this case. Also, we see the polarization response is problematic in the sense that, unlike the zenith incidence case, the linear combination of the x and y dipoles that yields pure LCP or pure RCP is now frequency-dependent.

Figure 5 shows the response at the active balun input, assuming a 100Ω input impedance, to a signal incident from $\theta = 74°$ and $\phi = 0$. Figure 6 shows the response at the far end of the cable for this scenario.

Figure 7 shows the open-circuit antenna response to a signal incident from $\theta = 74°$ (measured from zenith) and $\phi = 45°$; i.e., from a low-elevation azimuth half-way between the x- and y-oriented dipoles. Here we see the x-oriented dipole is sensitive to LCP, whereas the the $y-$oriented dipole response to LCP is significantly less. The responses of the $x-$ and $y-$oriented dipoles are exactly reversed for RCP. This can be explained as follows: For this orientation of the incident signal, each dipole appears as a crude approximation of one-half turn of a helix antenna, where the $x-$ and $y-$oriented dipoles appear to be "wound" in opposite directions. Thus, one is more sensitive to LCP and the other is more sensitive to RCP. Also, as in the case for $\phi = 0$, we see the polarization response is problematic in the sense that the linear combination of the x and y dipoles that yields

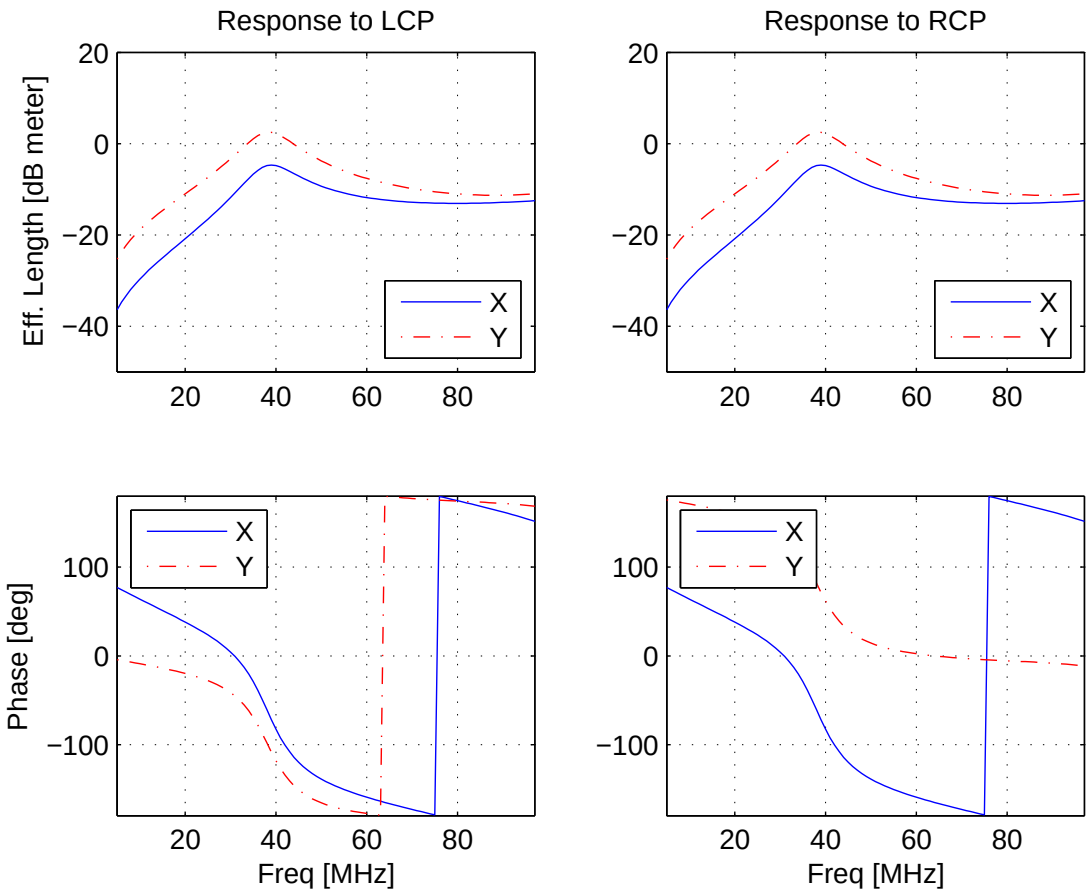

Figure 5: $\theta = 74°$, $\phi = 0$: Active balun input.

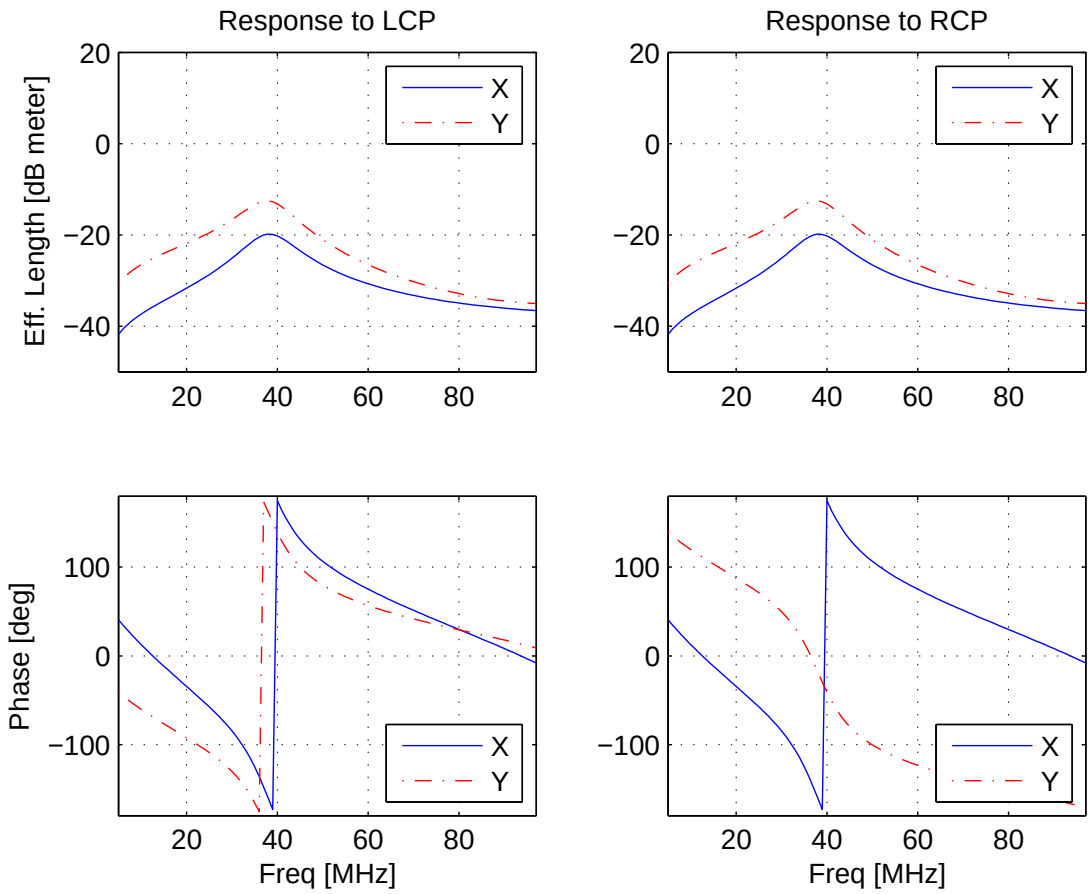

Figure 6: $\theta = 74°$, $\phi = 0$: Cable output.

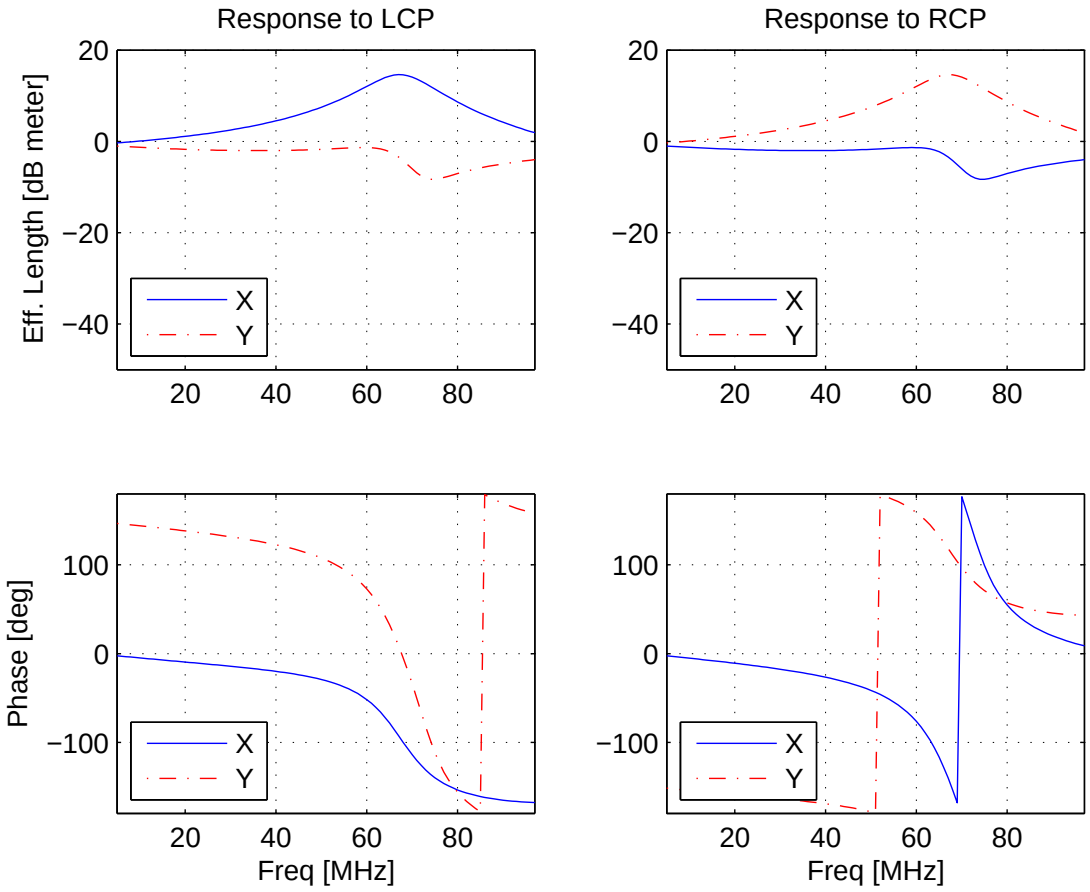

Figure 7: $\theta = 74°$, $\phi = 45°$: Open-circuit response.

pure LCP or pure RCP is frequency-dependent.

Figure 8 shows the response at the active balun input, assuming a 100Ω input impedance, to a signal incident from $\theta = 74°$ and $\phi = 45°$. Figure 9 shows the response at the far end of the cable for this scenario.

4 Efficacy of Polarization Calibration

Calibration of polarization can be defined as the process of converting the open circuit voltages V_x and V_y to voltages representing the LCP and RCP components of the incident electric field, E_L and E_R. From Equation 3, this can be done as follows:

$$\begin{bmatrix} E_L \\ E_R \end{bmatrix} = \left(\begin{bmatrix} (\hat{\mathbf{a}} \cdot \mathbf{l}_x) & (\hat{\mathbf{b}} \cdot \mathbf{l}_x) \\ (\hat{\mathbf{a}} \cdot \mathbf{l}_y) & (\hat{\mathbf{b}} \cdot \mathbf{l}_y) \end{bmatrix} \begin{bmatrix} 1 & 1 \\ j & -j \end{bmatrix} \right)^{-1} \begin{bmatrix} V_x \\ V_y \end{bmatrix} \tag{7}$$

For the purposes of this section of the memo we do not need to consider any other factors (e.g., impedance mismatch with the active balun or cable effects) since these affect both raw polarizations in exactly the same way.

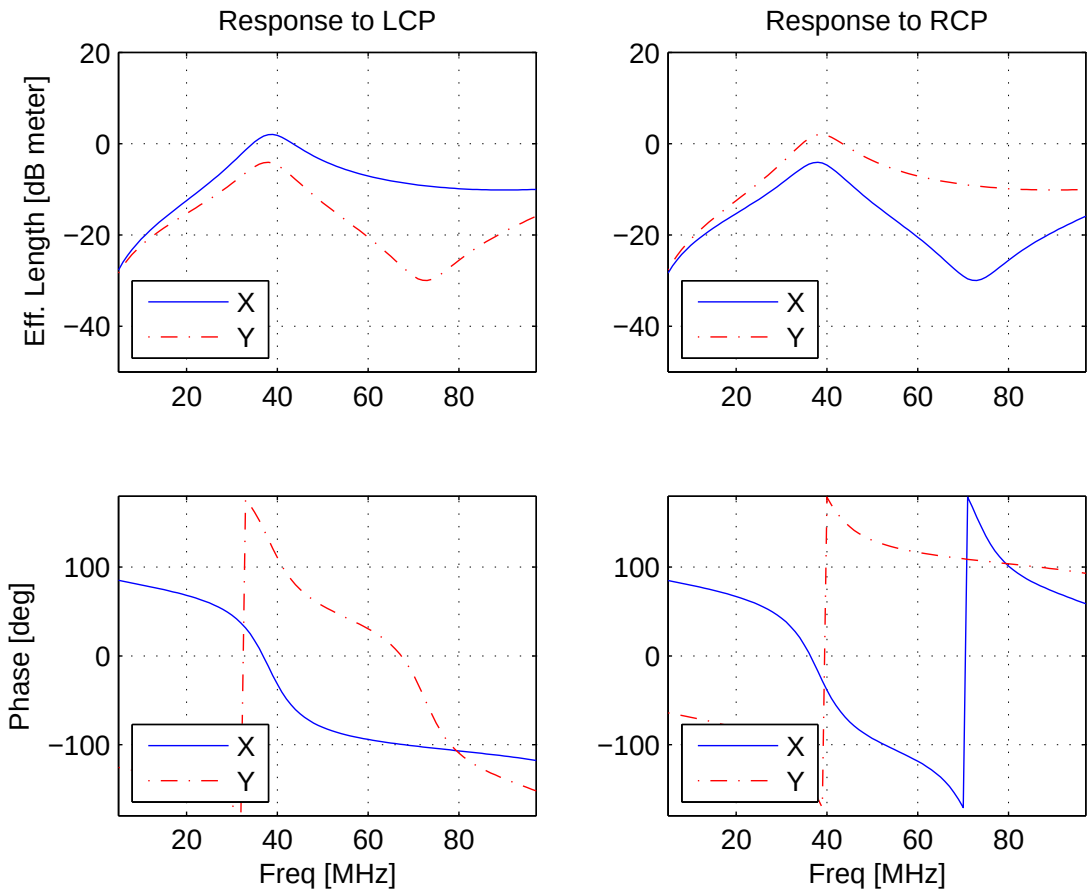

Figure 8: $\theta = 74°$, $\phi = 45°$: Active balun input.

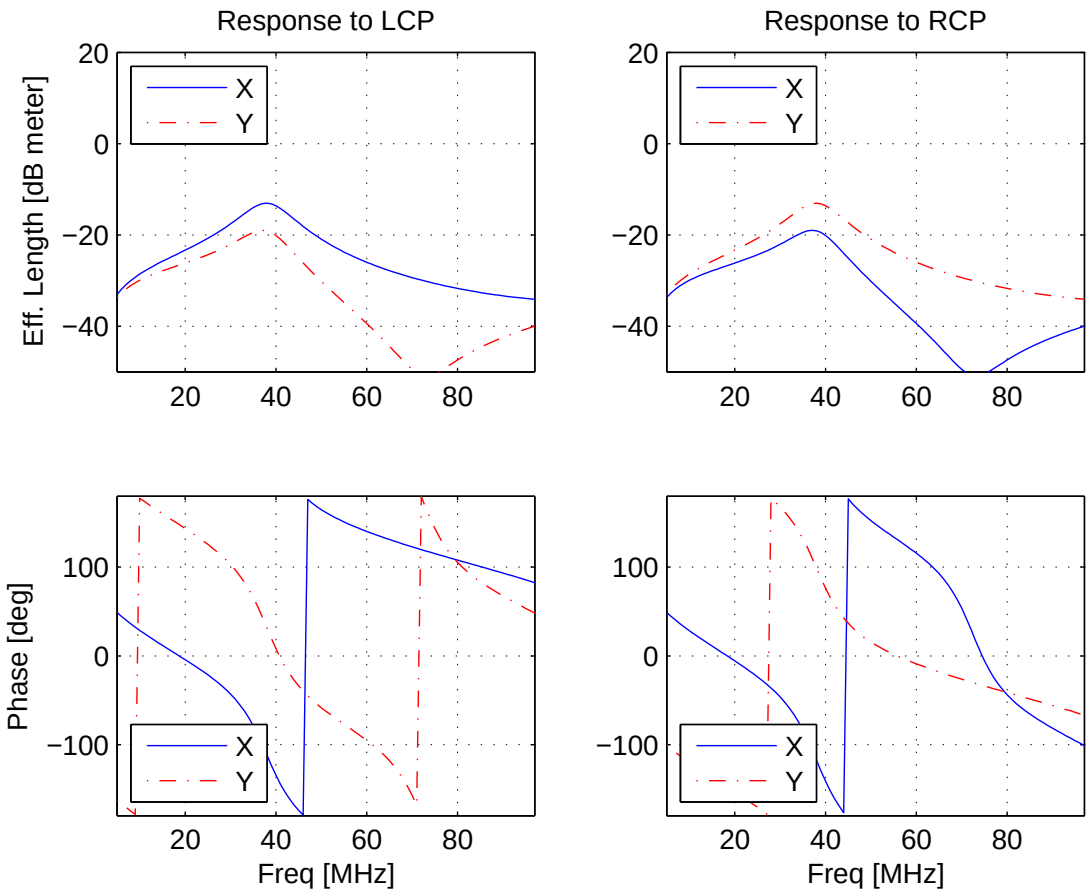

Figure 9: $\theta = 74°$, $\phi = 45°$: Cable output.

We now wish to consider the question of whether polarization calibration is always possible, or if there might be some conditions under which we can not recover pure LCP and RCP from the raw linears. The answer seems to depend on the matrix inversion in Equation 7. Let $\mathbf{P}$ be the matrix being inverted in Equation 7. Theoretically, $\mathbf{P}$ is invertible as long as it is not singular. In practice, $\mathbf{P}$ should also not be very close to being singular, in order to avoid numerical accuracy problems. A useful way to quantify the invertibility of $\mathbf{P}$ in this sense is in terms of the singular value ratio (SVR), which is defined for our purposes as the ratio of the smallest singular value of $\mathbf{P}$ to the largest singular value of $\mathbf{P}$. Ideally, SVR is 1, meaning $\mathbf{P}$ has full rank and is well-conditioned. On the other hand, if SVR is zero, then $\mathbf{P}$ has less than full-rank and cannot be inverted. Small values of $\mathbf{P}$ indicate that $\mathbf{P}$ has full rank and thus can be inverted, but with risk of numerical accuracy issues increasing with decreasing SVR. It is difficult to specify a minimum acceptable SVR, but certainly matrices with SVRs greater than 0.1 are safely invertible, and even matrices with SVRs orders of magnitude less are probably invertible assuming appropriate precautions are taken [6]. Thus, we can say that polarization calibration is theoretically possible if the SVR of $\mathbf{P}$ is greater than zero, and practical if the SVR of $\mathbf{P}$ is sufficiently large to allow numerically well-conditioned inversion.

Figures 10 and 11 show SVR for the scenario defined in the previous section as a function of θ and frequency for $\phi = 0$ and $\phi = 45°$, respectively. Note that the greatest risk (significantly low SVR) is limited to frequencies below 20 MHz and θ greater than about 80°. However there seems to be no case for which polarization calibration is completely out of the question.

It should be noted that the SVR is very closely related to axial ratio, so it should not be explicitly necessary to perform the above calculation in order to compare candidate antennas with respect to this criterion.

5 Effect of FIR Filter Length

As explained above (and elaborated in LWA Memo 106 [5]), perfect calibration is theoretically possible at a single frequency using a 2×2 matrix multiplication. To achieve this over a broad range of frequencies requires that each element of the matrix be expanded into a filter, as illustrated in Figure 1 of LWA Memo 106. In this section we assess the number of coefficients ("taps") and coefficient dynamic range required for these FIR filters. It is assumed that the *entire* response is to be calibrated, including not only polarization conversion but also correcting the effects of antenna mismatch and cable attenuation and dispersion. Specifically, we are considering the mathematical operation:

$$\begin{bmatrix} E_L \\ E_R \end{bmatrix} = \mathbf{Q}(\nu) \begin{bmatrix} \tilde{V}_x \\ \tilde{V}_y \end{bmatrix} \tag{8}$$

where $\tilde{V}_x$ and $\tilde{V}_y$ are obtained using Equation 6, ν is frequency, and $\mathbf{Q}(\nu)$ is an approximation (being implemented using *finite*-length filters) to the ideal calibration matrix:

$$\left(\frac{e^{-\gamma d}}{e^{-j\beta_0 d}} \frac{Z_L}{Z_A + Z_L} \begin{bmatrix} (\hat{\mathbf{a}} \cdot \mathbf{l}_x) & (\hat{\mathbf{b}} \cdot \mathbf{l}_x) \\ (\hat{\mathbf{a}} \cdot \mathbf{l}_y) & (\hat{\mathbf{b}} \cdot \mathbf{l}_y) \end{bmatrix} \begin{bmatrix} 1 & 1 \\ j & -j \end{bmatrix} \right)^{-1} \tag{9}$$

Note that the only effect remaining which is not considered here is the "ideal" portion of the cable delay. That portion of the calibration can be interpreted as part of the time-delay beamforming process, discussed in LWA Memo 107 [7].

The specific procedure followed in this section is as follows. For each scenario considered, we sample the forward model (Equation 6) to obtain $\tilde{V}_x$, $\tilde{V}_y$, and exact values for $\mathbf{Q}$ at 1 MHz intervals from 5 MHz to 98 MHz. The $\mathbf{Q}$ data are then extrapolated to obtain values for 1 MHz to 4 MHz (difficult to obtain directly due to numerical issues in the NEC model as the antenna becomes extremely small compared to a wavelength). The associated FIR filter coefficients are obtained by inverse discrete Fourier transform, yielding 98 coefficients per matrix element, suitable for a 98 MSPS (million

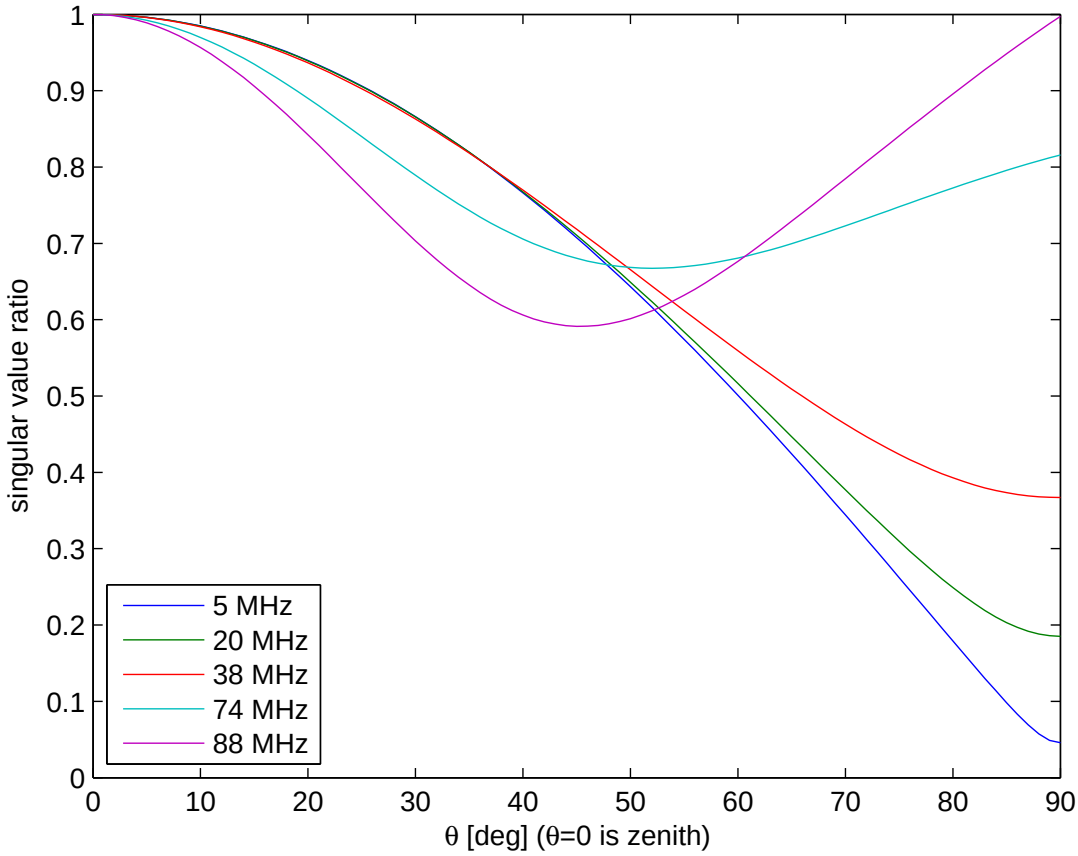

Figure 10: Efficacy of polarization calibration expressed in terms of singular value ratio; larger is better. $\phi = 0$.

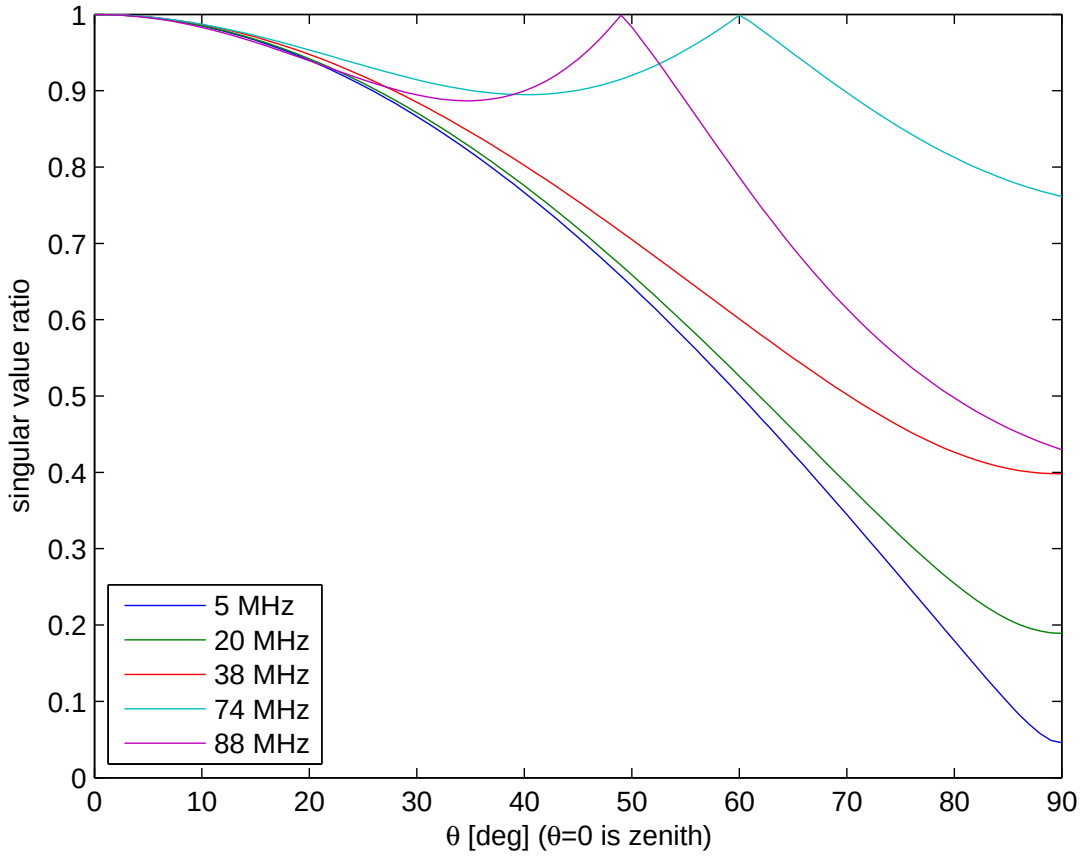

Figure 11: Efficacy of polarization calibration expressed in terms of singular value ratio; larger is better. $\phi = 45°$.

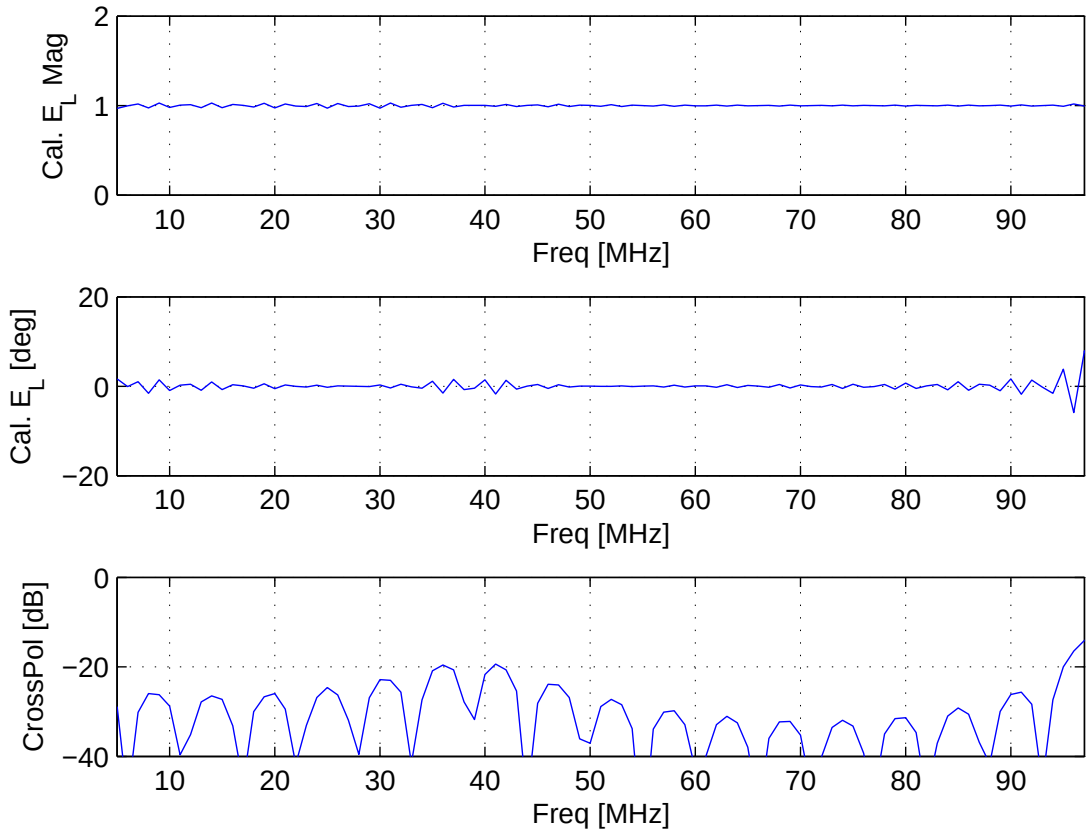

Figure 12: $\theta = 74°$, $\phi = 45°$: Calibrated LCP using $M = 80$ taps. Maximum tap dynamic range is 41 dB.

samples per second) complex-valued data stream. The number of coefficients is reduced to M by zeroing outer values. The performance is then determined by applying calibration to the sampled $\tilde{V}_x$ and $\tilde{V}_y$ using the truncated coefficient sets in the frequency domain.

The performance using $M = 80$ taps in the $\theta = 74°$, $\phi = 45°$ scenario is shown in Figure 12.[2] The top two plots show the magnitude and phase of the calibrated results, normalized such that a perfect result is 1 and 0° respectively. The lower plot is the cross polarization after calibration, which is defined here as the ratio of the undesired polarization (RCP in these examples) to the desired polarization (LCP). We see that for $M = 80$ the performance is quite good, although cross-pol rejection is limited to 20 dB over the frequency range of interest.

Figures 13, 14, 15, and 16 are the same results computed for $M = 32$, 16, 8, and 4 taps, respectively. Going forward, we shall use $M = 16$ only, assuming this represents a reasonable compromise between performance and computational effort. For $M = 16$, the worst-case cross-pol rejection is about -7 dB (irritatingly, at 38 MHz), although this value is closer to -15 dB to -20 dB over most of the frequency range of interest. Also it should be noted that it should be possible to shift "sweet

[2]Note there is no point in showing the result for $M = 98$ taps as this is guaranteed to be perfect due to the manner in which the simulation is designed. In practice, however, some error would exist. It is reasonable to assume that the error for smaller M is dominated by filter truncation.

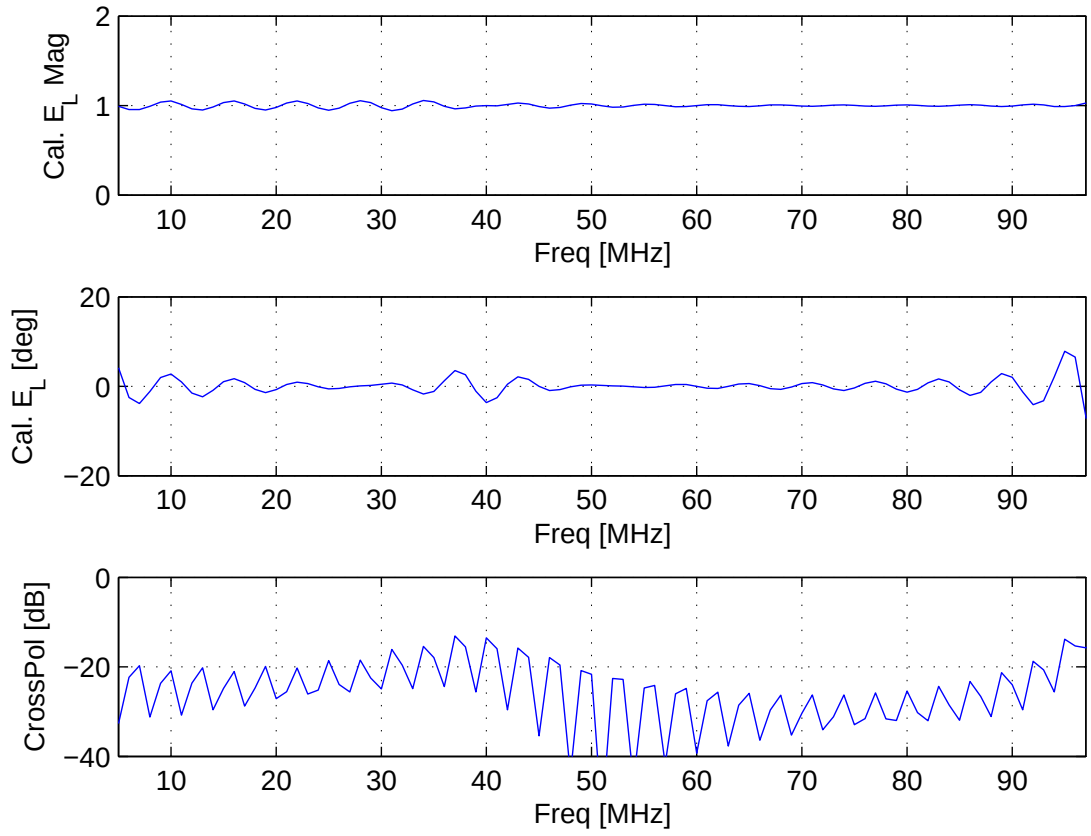

Figure 13: $\theta = 74°$, $\phi = 45°$: Calibrated LCP using $M = 32$ taps. Maximum tap dynamic range is 36 dB.

spots" in frequency to a limited extent, so the choice of $M = 16$ for the remainder of this memo should not be interpreted as a permanent degradation of 38 MHz. At $M = 16$ we also see that the maximum coefficient dynamic range, defined as the ratio of the magnitude of the largest coefficient to the magnitude of the smallest coefficient in any of the four FIRs, is 29 dB.

Figures 17 and 18 show the $M = 16$ results for $\theta = 74°$, $\phi = 0$ and $\theta = 0$ (zenith), respectively. The cross-pol for zenith calibration is always essentially perfect and does not depend on M.

6 Can We Just Calibrate to the Zenith?

The results in the previous section were computed assuming the ability to fine-tune the calibration for each direction of interest. In practice, it is highly desirable to be able to calibrate in one direction only – e.g., the zenith – and then to use the exact same calibration coefficients for all other directions. Clearly, this is reasonable for directions which are very close to the calibrated direction, but must degrade with increasing separation. A second consideration is that we would like some confirmation that a precise calibration for the beam center still applies at over the usable angular

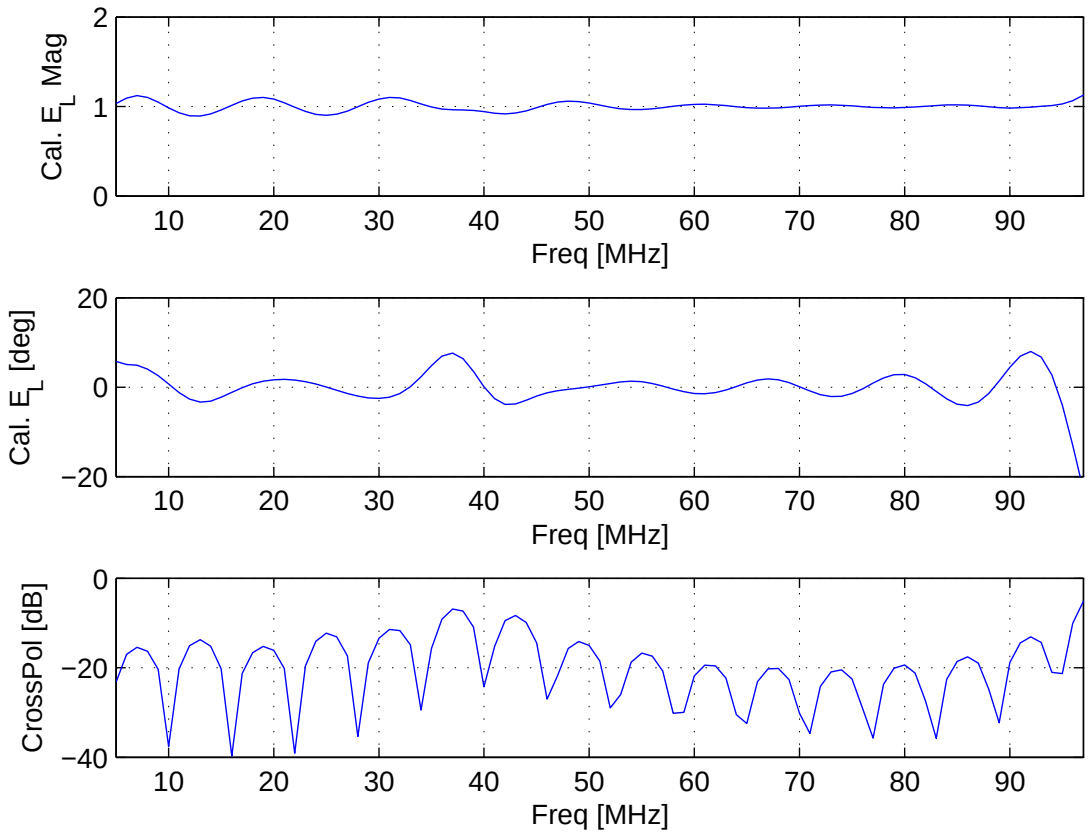

Figure 14: $\theta = 74°$, $\phi = 45°$: Calibrated LCP using $M = 16$ taps. Maximum tap dynamic range is 29 dB.

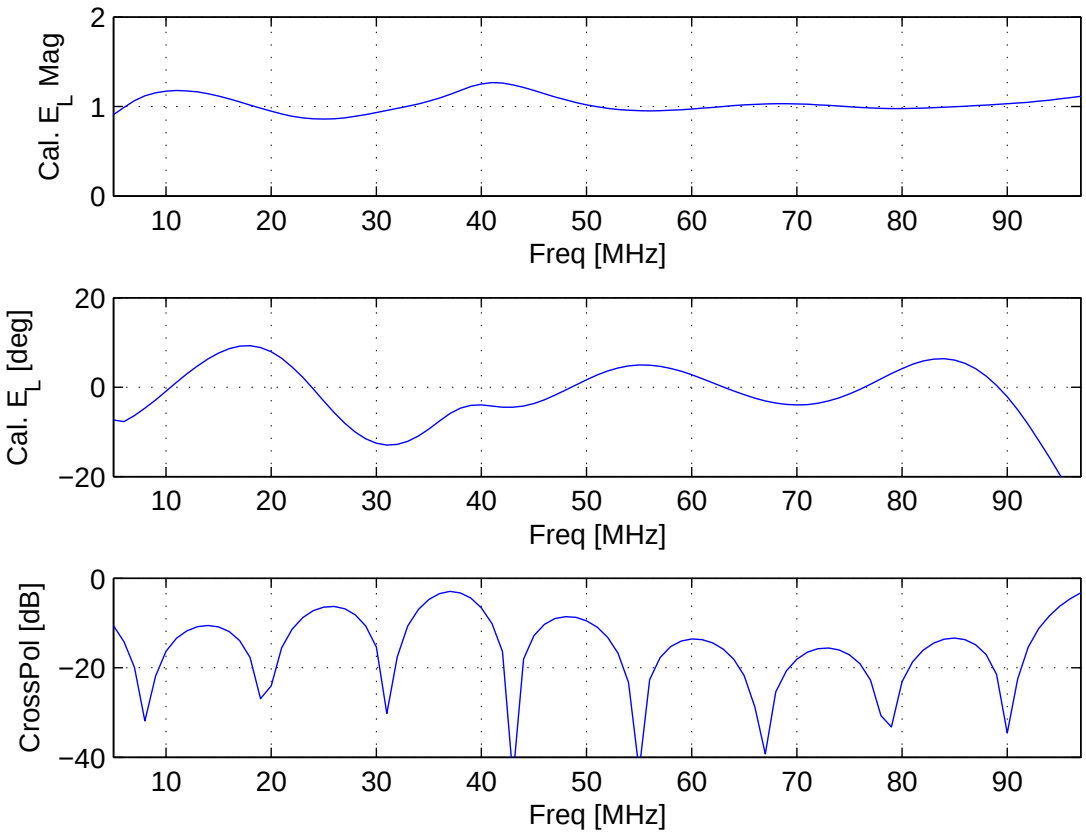

Figure 15: $\theta = 74°$, $\phi = 45°$: Calibrated LCP using $M = 8$ taps. Maximum tap dynamic range is 23 dB.

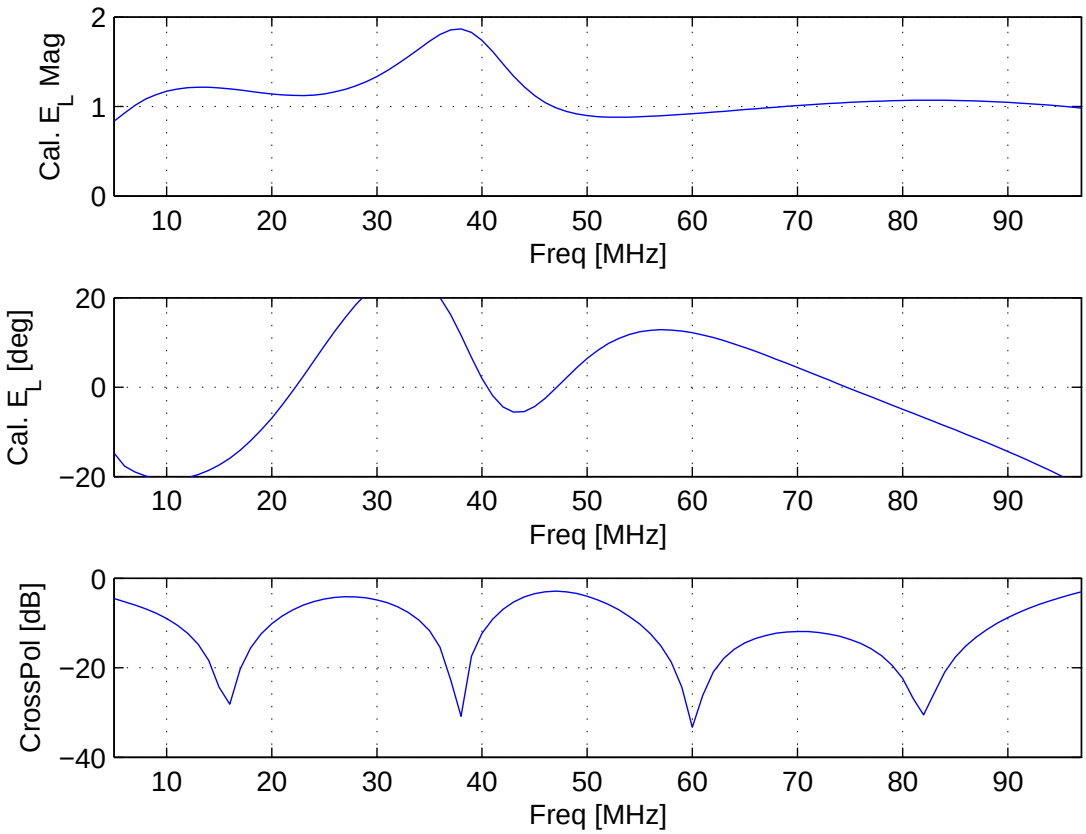

Figure 16: $\theta = 74°$, $\phi = 45°$: Calibrated LCP using $M = 4$ taps. Maximum tap dynamic range is 14 dB.

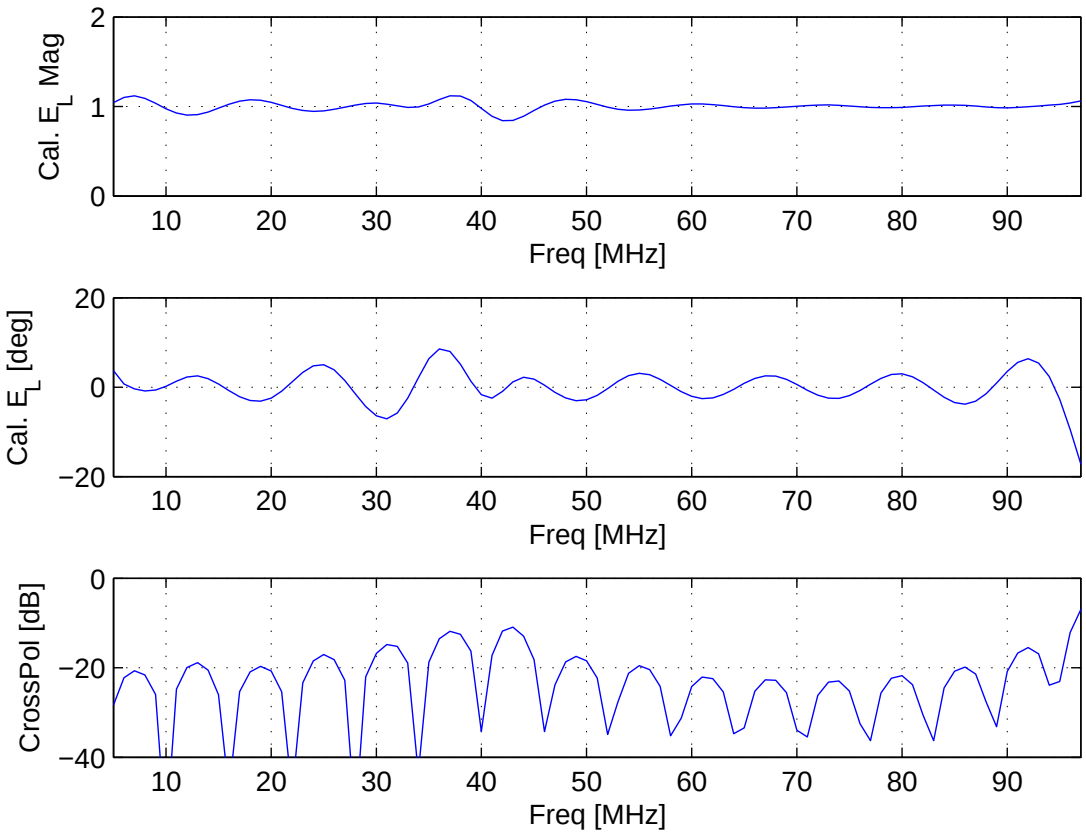

Figure 17: $\theta = 74°$, $\phi = 0$: Calibrated LCP using $M = 16$ taps. Maximum tap dynamic range is 36 dB.

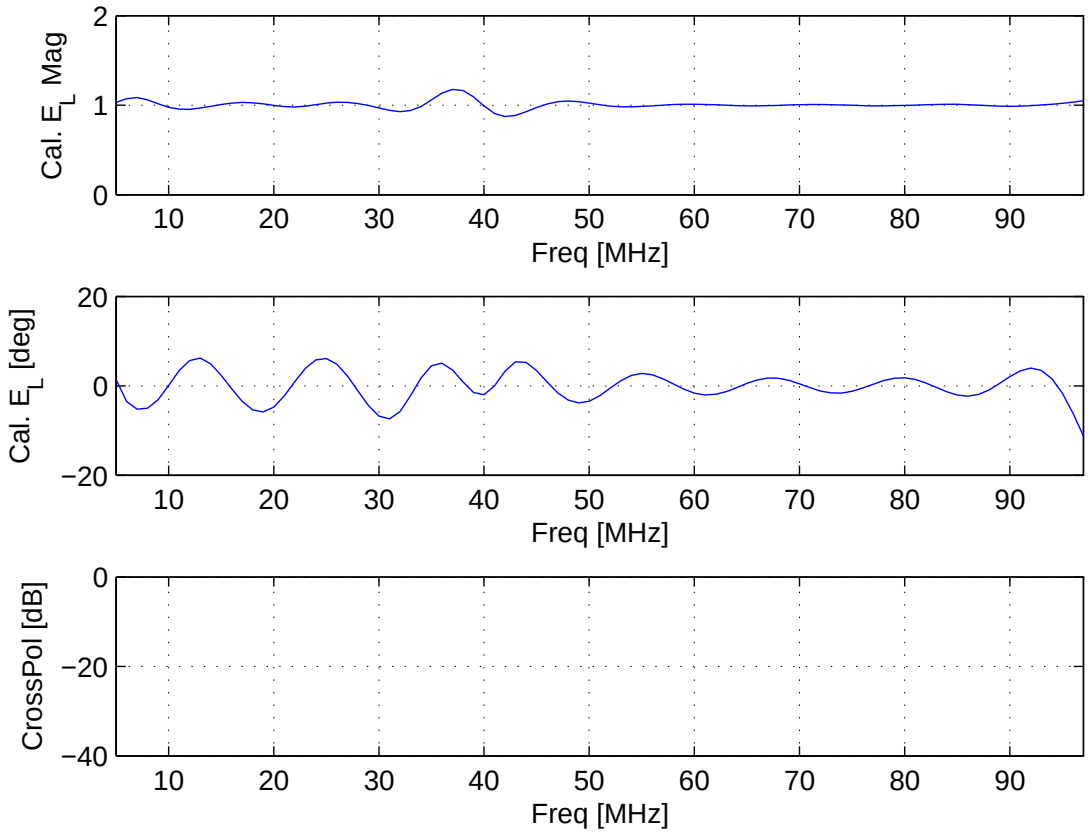

Figure 18: $\theta = 0$ (zenith), $\phi = 0$: Calibrated LCP using $M = 16$ taps. Maximum tap dynamic range is 32 dB. Crosspol in this case is effectively perfect (limited only by numerical precision).

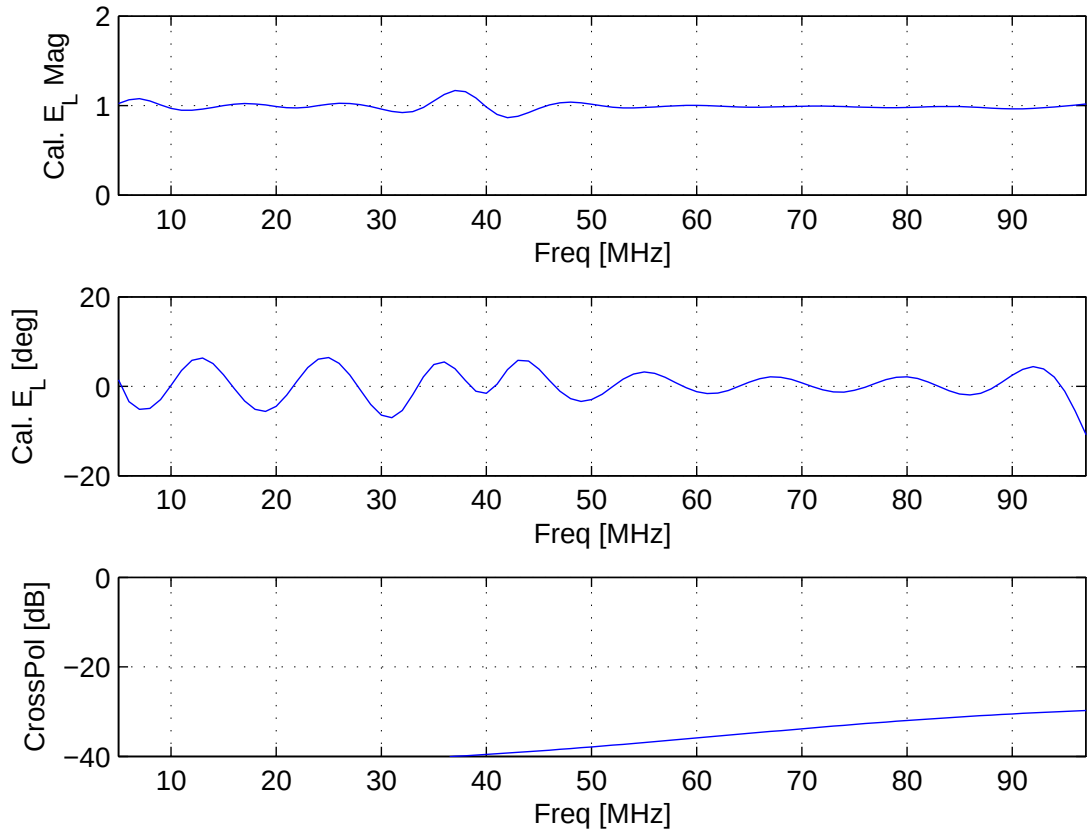

Figure 19: $\theta = 10°$, $\phi = 0$: Calibrated LCP using $M = 16$ tap solution for $\theta = 0°$.

extent of the beam (i.e., over the entire beam field-of-view).

Figure 19 shows the result when a calibration obtained for the zenith is applied to $\theta = 10°$, $\phi = 0$. As expected, there is some degradation (compare to Figure 18), in particular we see the cross-pol rejection creeping up at high frequencies. Figures 20, 21, 22, and 23 show the same results for $\theta = 30°$, $45°$, $60°$, and $74°$ respectively. We see that both the calibration accuracy and cross-pol rejection become seriously degraded between $45°$ and $60°$.

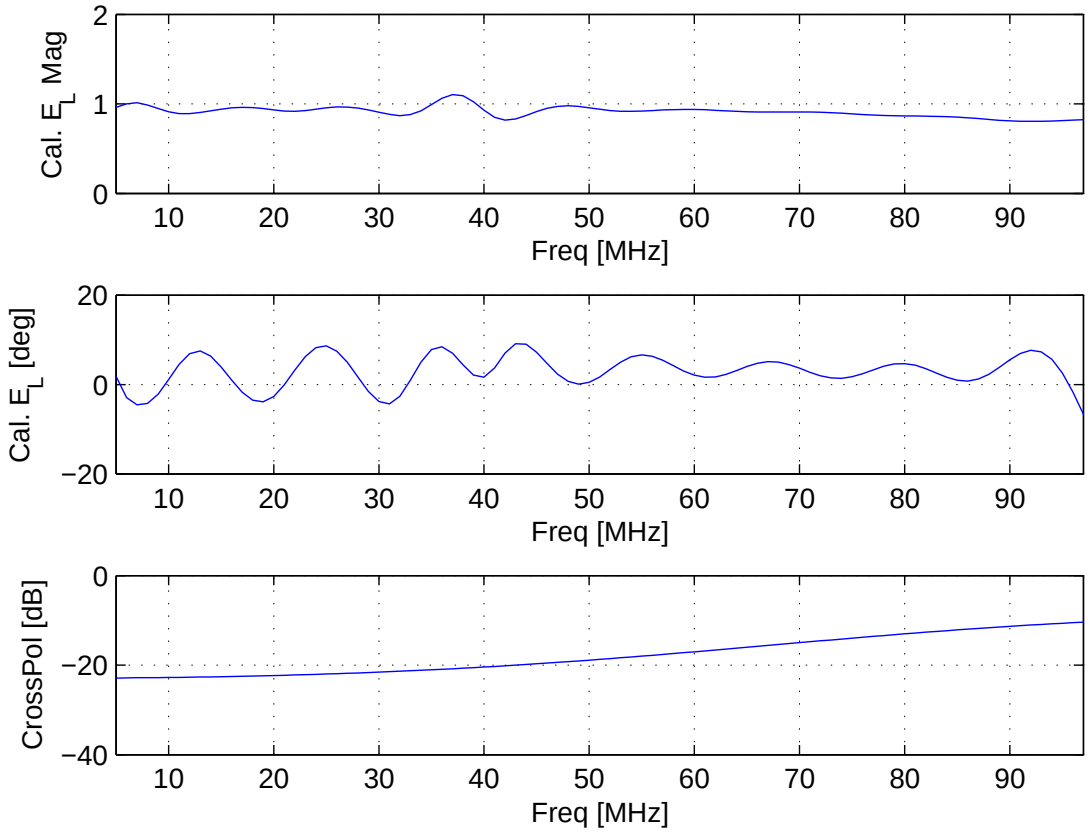

Figure 20: $\theta = 30°$, $\phi = 0$: Calibrated LCP using $M = 16$ tap solution for $\theta = 0°$.

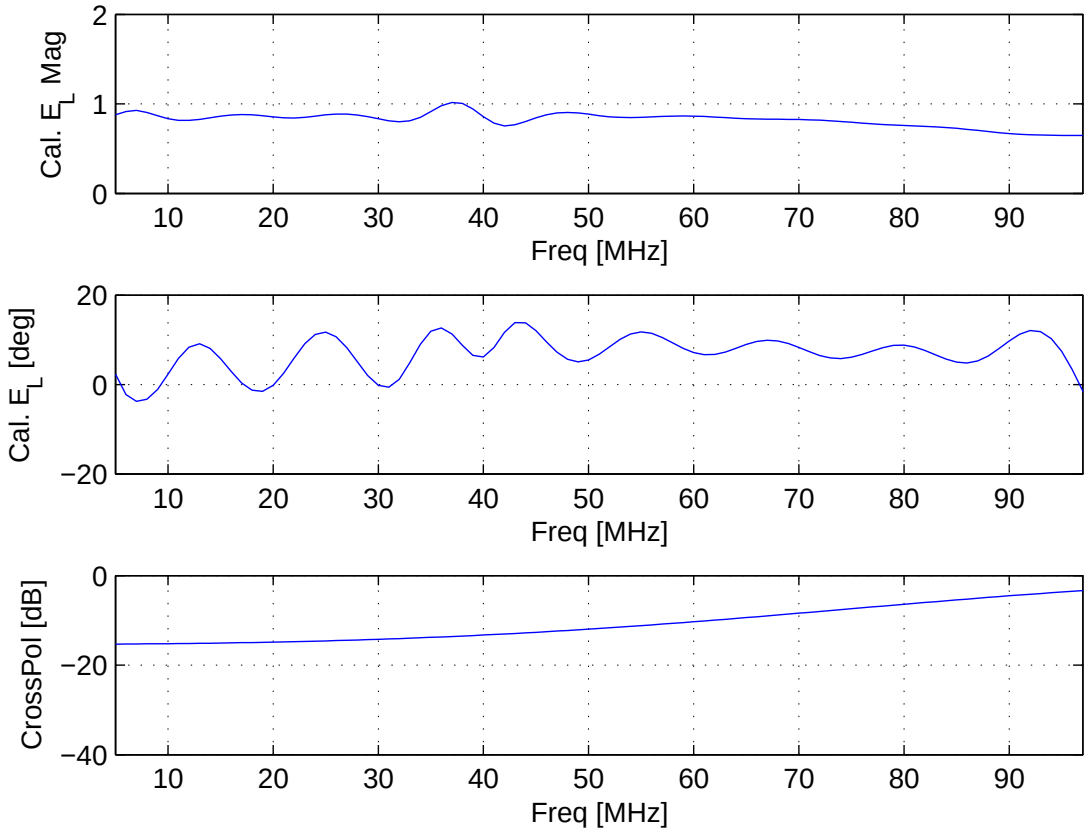

Figure 21: $\theta = 45°$, $\phi = 0$: Calibrated LCP using $M = 16$ tap solution for $\theta = 0°$.

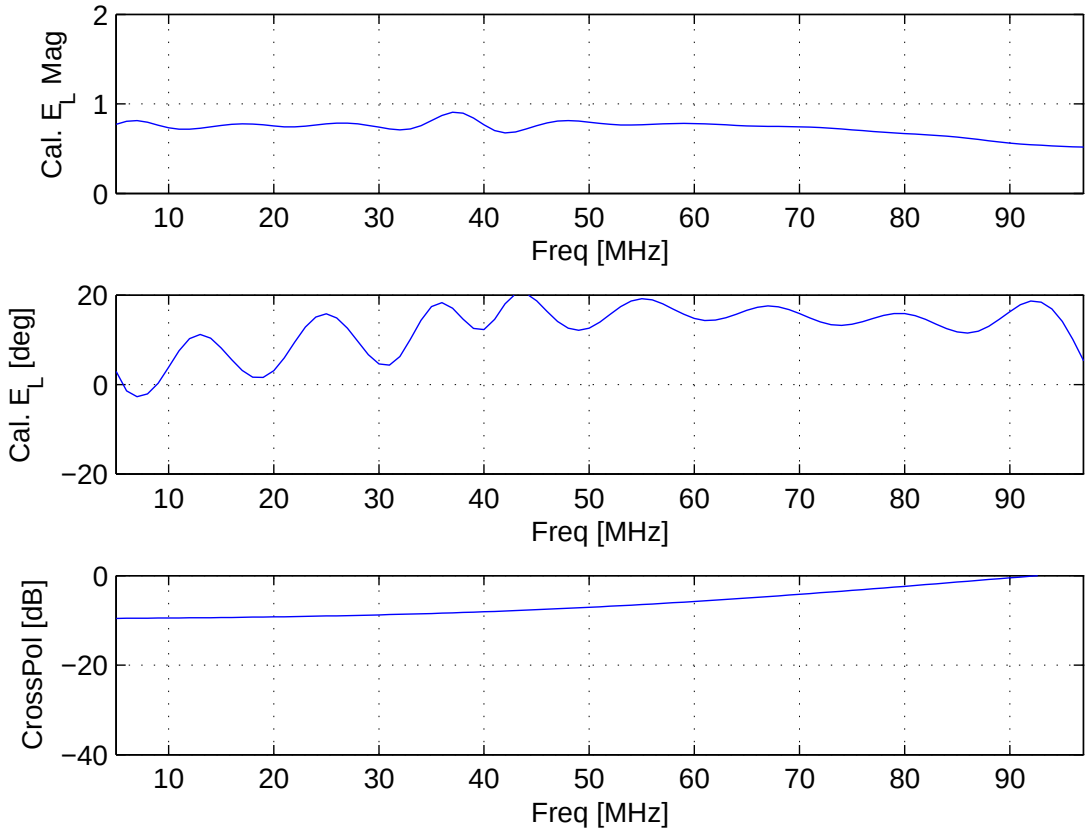

Figure 22: $\theta = 60°$, $\phi = 0$: Calibrated LCP using $M = 16$ tap solution for $\theta = 0°$.

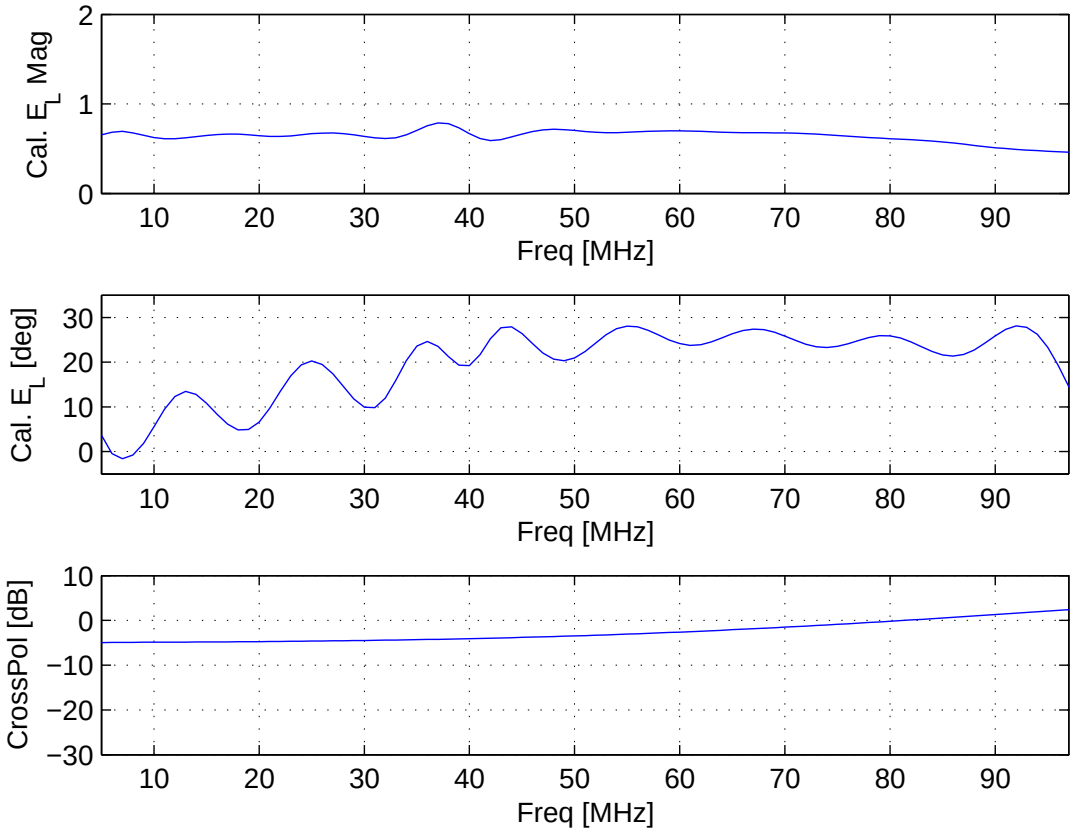

Figure 23: $\theta = 74°$, $\phi = 0$: Calibrated LCP using $M = 16$ tap solution for $\theta = 0°$. *Note modified scales in lower two plots.*

A NEC-2 Model & Input File

The NEC input file which defines the antenna used in this study follows:

```
CM Inverted V dipole with unit voltage source over a infinite PEC ground plane
CM Orthogonal dipole loaded with 100 ohm
CE
GW 1 12 -1.252  0.000 +0.298 -0.071  0.000 +1.510 0.015
GW 2  1 -0.071  0.000 +1.510 +0.071  0.000 +1.510 0.015
GW 3 12 +0.071  0.000 +1.510 +1.252  0.000 +0.298 0.015
GW 4 12  0.000 -1.252 +0.298  0.000 -0.070 +1.490 0.015
GW 5  1  0.000 -0.070 +1.490  0.000 +0.070 +1.490 0.003
GW 6 12  0.000 +0.070 +1.490  0.000 +1.252 +0.298 0.015
GE 1
GN 1
EK 0
EX 0 2 1 0 1
LD 4 5 1 1 100.0 0.0
FR 0 93 0 0 5.0 1.0
XQ
```

References

[1] S. Ellingson, "Long Wavelength Array Station Architecture" Ver. 1.0, Long Wavelength Array Memo Series No. 119, Nov 19, 2007. [online] http://www.phys.unm.edu/∼lwa/memos.

[2] A. Kerkhoff, "Comparison of Dipole Antenna Designs for the LWA," Long Wavelength Array Memo Series No. 102, August 25, 2007. [online] http://www.phys.unm.edu/∼lwa/memos.

[3] S. Ellingson, "Dispersion by Antennas," Long Wavelength Array Memo Series No. 115, December 11, 2007. [online] http://www.phys.unm.edu/∼lwa/memos.

[4] S. Ellingson, "Dispersion in Coaxial Cables," Long Wavelength Array Memo Series No. 136, Jun 1, 2008. [online] http://www.phys.unm.edu/∼lwa/memos.

[5] S.W. Ellingson, "Polarization Processing for LWA Stations," Long Wavelength Array Memo Series No. 106, October 29, 2007. [online] http://www.phys.unm.edu/∼lwa/memos.

[6] G.H. Golub and C.F. Van Loan, *Matrix Computations*, 3rd Ed., The Johns Hopkins University Press, 1996.

[7] S.W. Ellingson, "LWA Beamforming Design Concept," Long Wavelength Array Memo Series No. 107, October 30, 2007. [online] http://www.phys.unm.edu/∼lwa/memos.